Temporal and spatial variations in three-dimensional seismic oceanography

Zheguang Zou[1,2], Parsa Bakhtiari Rad[2], Leonardo Macelloni[3], and Likun Zhang[1,2]

[1]Department of Physics and Astronomy, University of Mississippi, University, MS 38677
[2]National Center for Physical Acoustics, University of Mississippi, 145 Hill Drive, University, MS 38677
[3]Hydrographic Science Research Center, School of Ocean Science and Engineering, The University of Southern Mississippi, 1020 Balch Blvd., Stennis Space Center, MS 39529

Correspondence: Likun Zhang (zhang@olemiss.edu)

Abstract. Seismic oceanography is a new cross-discipline between geophysics and oceanography that uses seismic reflection data to image and study ocean water columns. Previous works on seismic oceanography were largely limited to two-dimensional seismic data and methods. In this work, we explore temporal and spatial variations embedded in three-dimensional (3D) seismic oceanography. From a 3D multichannel seismic survey acquired for oil and gas exploration in the Gulf of Mexico over six months period, a 3D oceanic seismic volume was derived. The 3D seismic images exhibit both temporal and spatial variations of the ocean, and theoretical and empirical analyses were used to determine their contribution. Results suggest that temporal variation is largely embedded in the crossline direction, showing discontinuities due to acquisition at varied times; however, inline sections, which can be seen as snapshot representation of the water column, capture not only thermohaline structures but also temporal variation of ocean dynamics. Our findings highlight that marine 3D seismic data can provide superior oceanic images for the investigation of time-evolving mesoscale ocean dynamics.

1 Introduction

Despite being the Earth's largest habitat by volume, the ocean water column remains one of the most poorly explored environments. Even where investigations are executed, physical, biological, and chemical parameters are generally derived over one-dimensional (1D) profiles (e.g., CTD casts, buoys, and moorings) or two-dimensional (2D) transects (e.g., underwater gliders). Capturing the three-dimensional (3D) structure of the water column is extremely complicated: it can be reconstructed for a very large volume by combining 1D and 2D measurements, or, in a capacity limited for surface waters only, it can be inferred from satellite observations. Also, mesoscale and small-scale thermohaline fine structures are very difficult to observe with conventional methods whose lateral resolutions are coarse (usually > 100 m). The ocean interior instead is 3D by nature and varies in both time and space on a wide range of scales, as ocean dynamics such as internal waves, solitons, tidal beams, eddies and fronts (that affect thermohaline fine structures) are expected to vary both spatially and temporally.

Previous work has shown that marine seismic reflection profiling, a technique commonly used by geophysicists and geologists to image the Earth beneath the seafloor, can produce surprisingly detailed images of water-column structures. Holbrook et al. (2003) and Holbrook and Fer (2005) demonstrated that 2D seismic reflection sections, if appropriately processed, pro-

vided very high-resolution images of the ocean structure, both vertical and, in particular, horizontal. Within the ocean water column, water density variations, fine scale (1-10 m thickness) temperature-salinity contrasts, and water turbidity fluctuations result in small changes in sound speed that produce weak, but distinct, sound reflections. These reflections, 100 to 1000 times weaker than those from the solid earth below, have generally been neglected by geophysicists, whose focus is the structure of the sub-seafloor. However, studies reveal that these reflections correspond to ocean thermohaline structures (Nandi et al., 2004; Nakamura et al., 2006), and are primarily (not completely) associated with temperature gradient (Ruddick et al., 2009). This new cross-discipline, between exploration seismology and physical oceanography, has come to be known as seismic oceanography (Holbrook et al., 2003) and has been successfully applied to imaging mesoscale and sub-mesoscale water-column structures such as ocean fronts (Gorman et al., 2018), eddies (Song et al., 2009; Tang et al., 2014a), internal waves (Holbrook et al., 2009; Tang et al., 2014b; Buffett et al., 2017), and other thermohaline fine structures (Holbrook et al., 2003). Additionally, several theoretical studies have been derived from the application of water-column seismic images including estimation of geostrophic currents (Sheen et al., 2011; Tang et al., 2014b), wave field spectra (Fortin et al., 2016), and internal wave mixing (Dickinson et al., 2017). Most of these studies used 2D seismic data and processing methods, but, in the modern exploration seismology of the oil and gas industry, 2D seismic methods are gradually upgraded to 3D seismic methods, which provide more adequate seismic images with the help of the additional dimension, leading to a more reliable interpretation (Yilmaz, 2001).

3D seismic surveys are distinguished from 2D seismic surveys by the contemporary acquisition of multiple closely spaced lines (e.g., 25 m) that provides regular data point spacing. This leads to a true data volume from which lines, planes, slices, or probes can be extracted in any orientation, with nominally consistent data processing characteristics. While it is possible to acquire a dense, high-resolution grid of 2D lines, such grids are fundamentally different from a native 3D seismic survey (Lonergan and White, 1999; Yilmaz, 2001). The close spacing of 3D seismic lines and the physical illumination of the subsurface from multiple offsets and multiple azimuths remove spatial aliasing problems inherent to 2D seismic data, therefore 3D seismic oceanography has the potential to yield better spatial resolution and can be useful for studying the orientation of ocean structures (Blacic and Holbrook, 2010). To date, 3D seismic oceanography is still not well developed, which can be due to multiple facts: the 3D seismic data are very expensive to acquire, there is an interdisciplinary gap between oceanography and geophysics, and most importantly, a fundamental understanding of the capability of 3D seismic oceanography is missing.

The fundamental principle of exploration seismology assumes prevalently only spatial and not temporal variations in the subsurface (at least in the survey time frame). However, this challenges the development of 3D seismic oceanography, as 3D seismic surveys are generally acquired over a long period (e.g., from hours to months) and the water column may evolve during the collection of 3D seismic data. Very recently, 3D seismic oceanography moved a big step forward, successfully being applied to explore the evolution of a front (Gunn et al., 2020) and the passage of an eddy (Dickinson et al., 2020). However, there are still many fundamental questions regarding 3D seismic oceanography waiting to be answered. For example, how are temporal and spatial water-column variations distributed in a single 3D seismic volume? Can we quantify them? Is the oceanic 3D seismic imaging meaningful in all directions? The answers to these questions will be useful to guide the development of future 3D seismic oceanography.
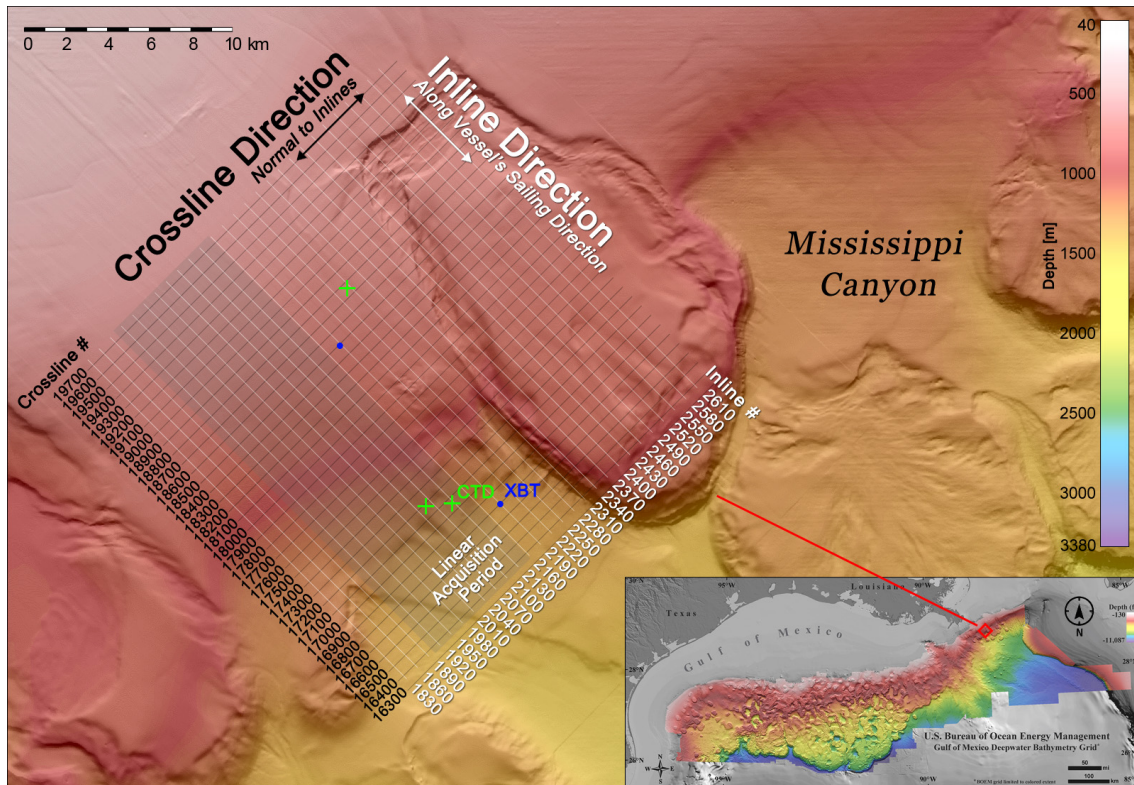
Figure 1. 3D seismic survey area with inline (white) and crossline (black) configuration, CTD (green cross) and XBT (blue dots) locations, and seafloor topography (background color). The 3D seismic survey area is marked by the grids. Inline is oriented to go down the continental slope. The inset shows the survey location in the Northern Gulf of Mexico. The seafloor topography data are provided by Bureau of Ocean Energy Management. The grey grids mark the linear acquisition period (explained in Sec. 2.4).

In this study, we explore temporal and spatial variations embedded in 3D ocean seismic volume and answer the fundamental questions mentioned above. We report results of a 3D seismic oceanography study carried out at the continental slope region of the northern Gulf of Mexico, where seismic imaging of ocean structures can be useful for understanding ocean dynamics and mixing. We analyzed multi-directional (inline, crossline, and depth-slice) seismic images to reveal fundamental imaging features. We further conducted theoretical and empirical analyses to understand the distribution of temporal and spatial variations. This new understanding will be useful for the interpretation of 3D seismic data as spatio-temporal evolution of ocean interior structure, which is important to promote the development of 3D seismic oceanography.

2 Data and Methods

2.1 3D Seismic Data

The seismic data used in this study are a portion of a large multichannel 3D seismic survey conducted by Schlumberger WesternGeco in the Northern Gulf of Mexico for oil and gas exploration between 2002 and 2003. Our study region (Fig. 1) is at the continental slope of the northern Gulf of Mexico, outside the Mississippi River delta, where the water dynamics in this region is mainly dominated by the Loop Currents and the Mississippi River outflows (Coleman, 1988; Sturges and Lugo-Fernandez, 2005). Although our seismic region is a bit far north of the Loop Currents, it is still a high eddy-kinetic energy region due to eddies and jets over the continental slope (Hamilton and Lee, 2005). Seismic surveying lines run from northwest to southeast (inline azimuth, 330°) over a gentle continental slope (average inclination, 1.5°) where the seabed depth ranges from 800 m to 1300 m. Seismic data were collected using 2 airguns of 5085 cubic inches each in flip-flop configuration and 8 streamers, each accommodating 640 hydrophones. The streamer spacing was 100 m, and the hydrophone spacing was 12.5 m. We received the raw shot gathers sampled at 2 milliseconds (ms) and cut at the seafloor with no processing applied apart from analog to digital anti-aliasing filtering (frequency range, 3-200 Hz). We received multiple CTD and XBT casts, including three CTD and two XBT casts inside the seismic area (see Fig. 1).

2.2 3D Seismic Data Processing

Imaging the ocean water column using 3D seismic data from the oil industry is challenging. Acquisition geometry is not optimized for this target, and ocean internal reflections are inherently weak and masked by noises of different nature. However, oil industry contractors employ cutting-edge technology and therefore the obtained seismic data are generally of very high quality. The seismic data processing was started with trace editing and amplitude balancing. We have removed offsets greater than 4 km (half of the total channel number) to keep computational costs low, and to reduce the effect of long-offset deviations on the data preprocessing and velocity model building. The strong seafloor reflections were also muted to achieve a relative balance of amplitude levels. The data preprocessing used here employed standard techniques for subsurface seismic imaging, described in Yilmaz (2001), adapted to work with the water-column specific issues. Typical marine noises were present in the water-column data, e.g., acquisition-related noise, direct arrivals, reflection energy returns from previous shots, etc. Environmental noises include wind, shipping activity, and inherent ocean noise. We designed a filtering strategy specifically tailored to remove or minimize as much noise as possible while preserving the weak signals of interest. Consequently, we used low-cut 5 Hz and high-cut 150 Hz Butterworth filtering after each processing flow in various data domains to attenuate noise. The direct waves overlapped the subtle internal reflections of the water column and complicated the imaging. We applied frequency-wavenumber (FK) filtering and Radon filtering in different data domains to fruitfully attenuate unwanted linear noise, previous shot multiples, and seafloor refraction.

We processed the 3D data in a 3D fashion (which uses both inline and crossline data), rather than sequential 2D processing. The spherical divergence was compensated using the conventional exponential gain function (with a power of 2) after some trials. For velocity analysis and normal move-out (NMO) correction, the data sort was changed to common-midpoint (CMP)

and the semblance panels were produced in a window of 1410 to 1590 m/s. To build a reliable velocity model, sound velocities derived from CTD measurements were used to calibrate the seismic velocity model when there is a big mismatch between model and measurement. Afterward, high coherence semblances were picked manually in a distance interval of every 250 m in both directions to model root-mean-square (RMS) velocities for further processing. The CTD casts are high-resolution data and hence are helpful for quality control of velocity model building. In this sense, the CTD is used as guidance for the manual picking of the semblance panels. Accordingly stacking and time migration were performed using the RMS velocities to produce interpretable seismic images.

We have also tested and performed a powerful multi-parameter imaging technique known as the common-reflection-surface (CRS) method for stacking and enhancing the data and also to avoid the NMO stretch effect (Yilmaz, 2001). The size of the CRS stacking surface was however chosen conservatively small, in particular in the crossline direction (50 m), to avoid stacking traces from different swaths. The CRS showed improved results compared to the conventional CMP-based imaging especially along the inline direction (Bakhtiari Rad and Macelloni, 2020). Afterward, post-stack time migration was performed using the estimated RMS velocities to correct the dipping events. Finally, the data were time-to-depth converted using the estimated velocity function integrated with in situ sound velocity casts. More details of our seismic processing can be found in Bakhtiari Rad and Macelloni (2020).

2.3 3D Seismic Volume

The obtained 3D seismic volume of the ocean interior is illustrated in Fig. 2, showing the "slicing" configuration of 3D inline, crossline, and depth-line seismic images. A 3D seismic volume is generally a 3D matrix in which seismic reflections are color-coded according to the reflection amplitude and polarity. Each seismic reflection in seismic images represents an "interface" between two water layers with different acoustic impedances, stemming from different temperature and salinity in the water column (Ruddick et al., 2009). Because a seismic survey can be acquired in any planar directions, the notation in geographic coordinates (i.e., latitude and longitude) is not adopted. Instead, the planar position is organized in *inline* (the direction; down the continental slope) and *crossline* (perpendicular to inline; the northeast-southwest direction; along the continental slope on a broad scale); see Figs. 1 and 2. The volume has a spatial resolution of 6.25 m in the inline direction, 25 m in the crossline direction, and 6-7 m in the vertical direction (assuming a sound speed of 1500 m/s and considering the dominant frequency of the airgun signal in the water column between 50 and 60 Hz). Our seismic volume shows only the portion of the water column below 200 m because the geometry of sources and receivers, optimized for deep subsurface targets (several kilometers below the seafloor), poorly image the shallowest portion of the water column (Piété et al., 2013). The signal-to-noise ratio (SNR) of our inline seismic images is ranging from 8-10, using the formula of Holbrook et al. (2013).

It is important to note that for a 3D seismic oceanography study, inline sections are often acquired during short temporal intervals (typically a few hours considering the normal vessel velocity of 2.5 m/s). However, crossline sections, which are obtained interpolating the inline sections perpendicularly, may embrace a wide temporal interval (from a few hours up to several months; the average interval is about 8 hours within the linear acquisition period). We assume that water-column reflectors do not move during the shot and the signal recording (the stick-slip model assumption (Klaeschen et al., 2009)).
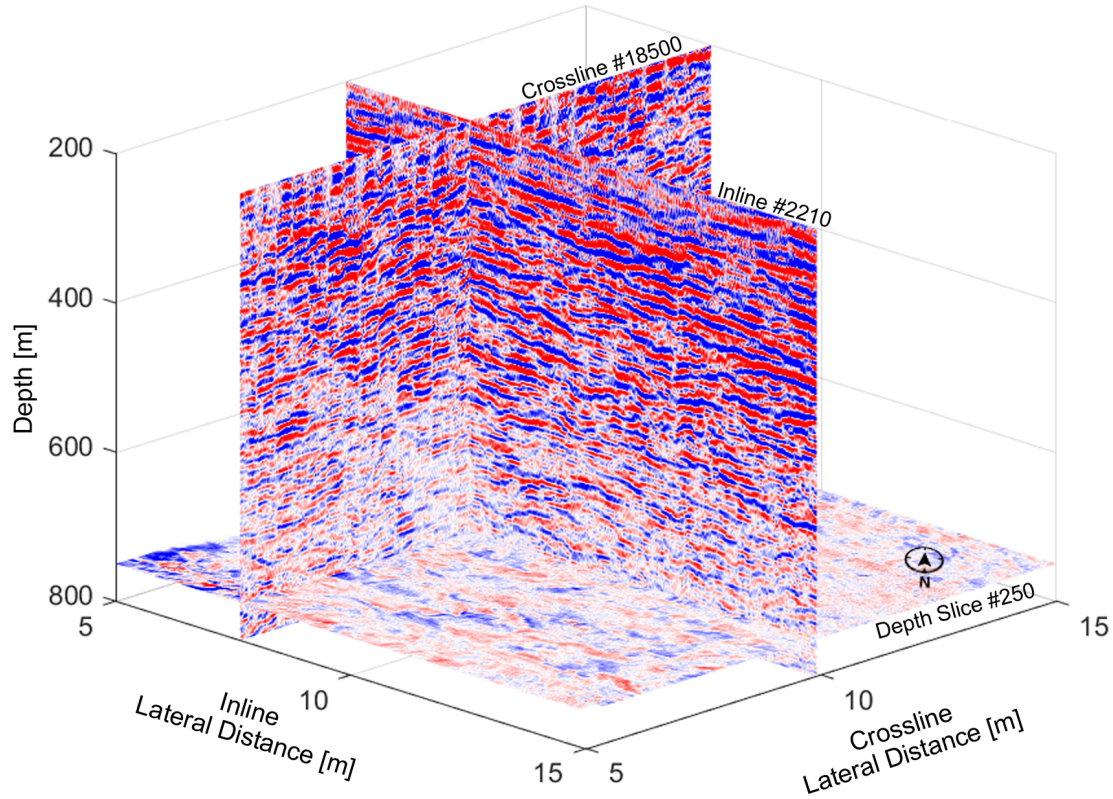
Figure 2. The inline, crossline and depth-slice configuration in our obtained water-column 3D seismic volume in the Gulf of Mexico. The lateral resolutions in inline and crossline directions are 6.25 m and 25 m, respectively, and the vertical resolution is 6-7 m. The color represents the amplitude of seismic reflection.

Considering our inline collection time (a few hours) is smaller than the timescale of the mesoscale ocean dynamics (days), we assume that each inline represents a seismic snapshot of the water column. The entire 3D seismic volume extends for 480 km^3 of the water column in the Gulf of Mexico. It consists of 821 inline sections, 3,463 crossline sections, and 256 depth slices. Temporally, it covers over six months, from August 2002 to February 2003, with most collected between September and October.

2.4 Imaging Capability Analysis

To test if the 3D volume properly images the water column structures, we compared the seismic reflections with acoustic reflection coefficient derived by inverting the temperature-salinity curves collected along with the CTD profiles (Nakamura et al., 2006). The acoustic reflection coefficient for normal incident sound waves is given by (Kinsler et al., 1999):

$$R_s = \frac{\rho_1 c_1 - \rho_0 c_0}{\rho_1 c_1 + \rho_0 c_0} \tag{1}$$
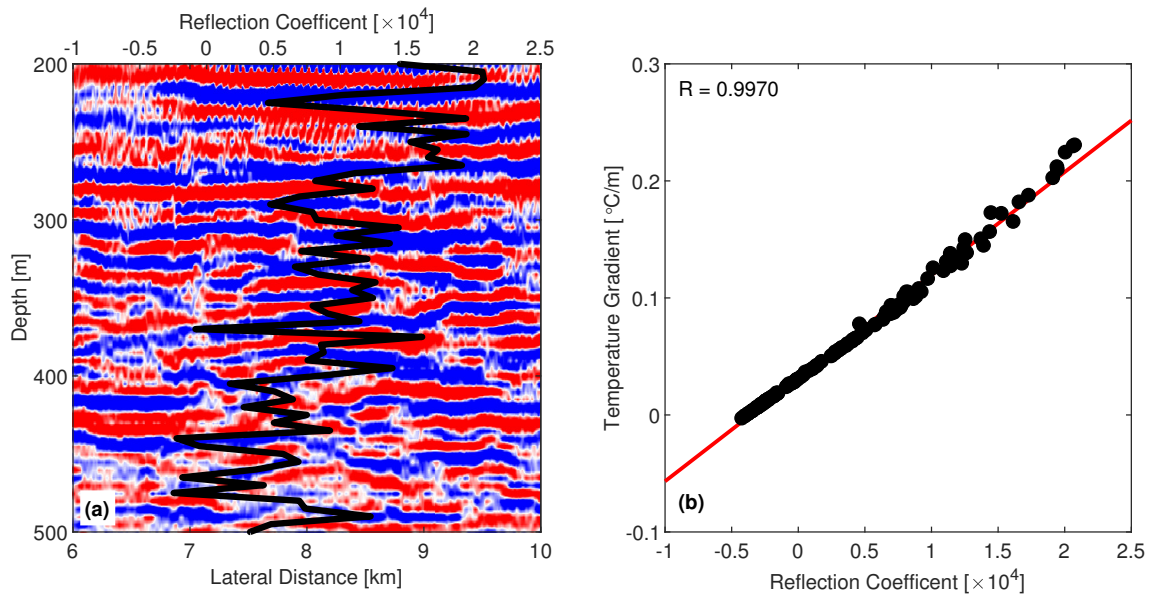
Figure 3. (a) Comparison of seismic imaging (Inline 2130) and the derived reflection coefficient (curve) from CTD data, both acquired on October 17, 2002. (b) Correlation between temperature gradient and the derived reflection coefficient between 200-1000 m.

where ρ_0, ρ_1 and c_0, c_1 are density and sound speed; the subscripts 0 and 1 specify adjacent layers. It has been widely demonstrated that the amplitude of seismic reflections is largely related to temperature gradients in the water column (Nandi et al., 2004; Nakamura et al., 2006; Ruddick et al., 2009), but sometimes salinity may play a role up to 40% in regions prone
145 to diffusive convection (Sallarès et al., 2009). Figure 3 (a) compares the reflection coefficient derived from concurrent CTD measurements (collected on October 17, 2002, location shown in Fig. 1) with our seismic imaging (Inline #2130; seismic data collected on October 17, 2002). The overall agreement between the derived reflection coefficients with the seismic reflections suggests that our 3D seismic data successfully represents water-column thermohaline structures. Also, the derived reflection coefficient correlates highly ($R = 0.9970$) with the temperature gradient [Fig. 3 (b)], suggesting that the seismic amplitude in
150 our seismic images can be interpreted as the vertical temperature gradient of the water column. In addition, the depth of the 3D volume seafloor reflection matches within 5-10 m error the seafloor depth from multibeam bathymetry which is derived using very high accurate sound speed measurements collected by NOAA's Ship Okeanos Explorer, confirming that our migration is accurate and our seismic images accurately represent the water column structure.

2.5 Survey Line Analysis

155 Once we have established the oceanic natures of the seismic reflections, we resolve the correct relationship between time and space within our 3D seismic volume. We emphasize that inline sections are generally acquired during a short temporal interval (typically a few hours considering the normal vessel velocity of 2.5 m/s), while crossline sections, which are obtained by interpolating the inline sections perpendicularly, embrace a wide temporal interval, in our case up to several months. It has
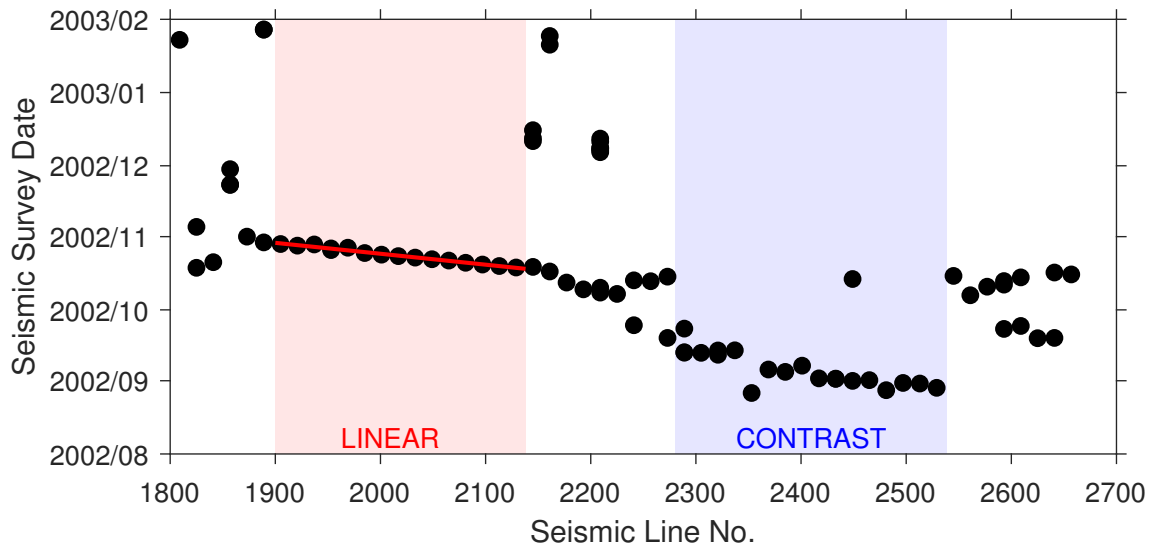
Figure 4. Dates of the seismic survey for the survey lines analyzed in our work. Two highlighted periods are a linear acquisition period (Lines # 1900-2140) during which data were collected linearly in time and space intervals, and a contrast acquisition period (Lines #2280-2540) which can display a huge time jump in seismic image. The line number here is equivalent to the inline number at the center of a seismic swath.

been demonstrated that water-column reflectors do not move during the very short time between the shot and the recording of
160   the reflected signal (Klaeschen et al., 2009). In 3D surveys each shot is recorded simultaneously along with parallel streamers, generally referred to as swaths, which for our data set count 8 streamers. To better understand the temporal distribution of the inline/swath, we carefully investigate the acquisition time for each survey line by referring to the field acquisition records.

Figure 4 shows the seismic line number, which is equivalent to the center inline number of a seismic swath, as a function of the recording date and time. Considering that 3D surveys are ideally carried out by acquiring adjacent swaths consecutively,
165   we should observe a linear relationship between sailing line number and survey time. However, it is common that owing to operational problems (e.g., weather, maritime traffic, etc.) and/or bad data acquisition some portion of the area may be covered at a different time or some lines may be reacquired. Figure 4 shows a general linear trend, in particular for the portion including Lines 1900-2140. In this interval, spatially contiguous seismic lines were collected consecutively in time, yielding a crossline surveying speed of 1.5 swath per day (equivalent to 0.6 km crossline imaging per day). We refer to this portion as *linear*
170   *acquisition period* and we will use it in the correlation analysis discussed further.

3   Results

3.1   3D Oceanic Seismic Images
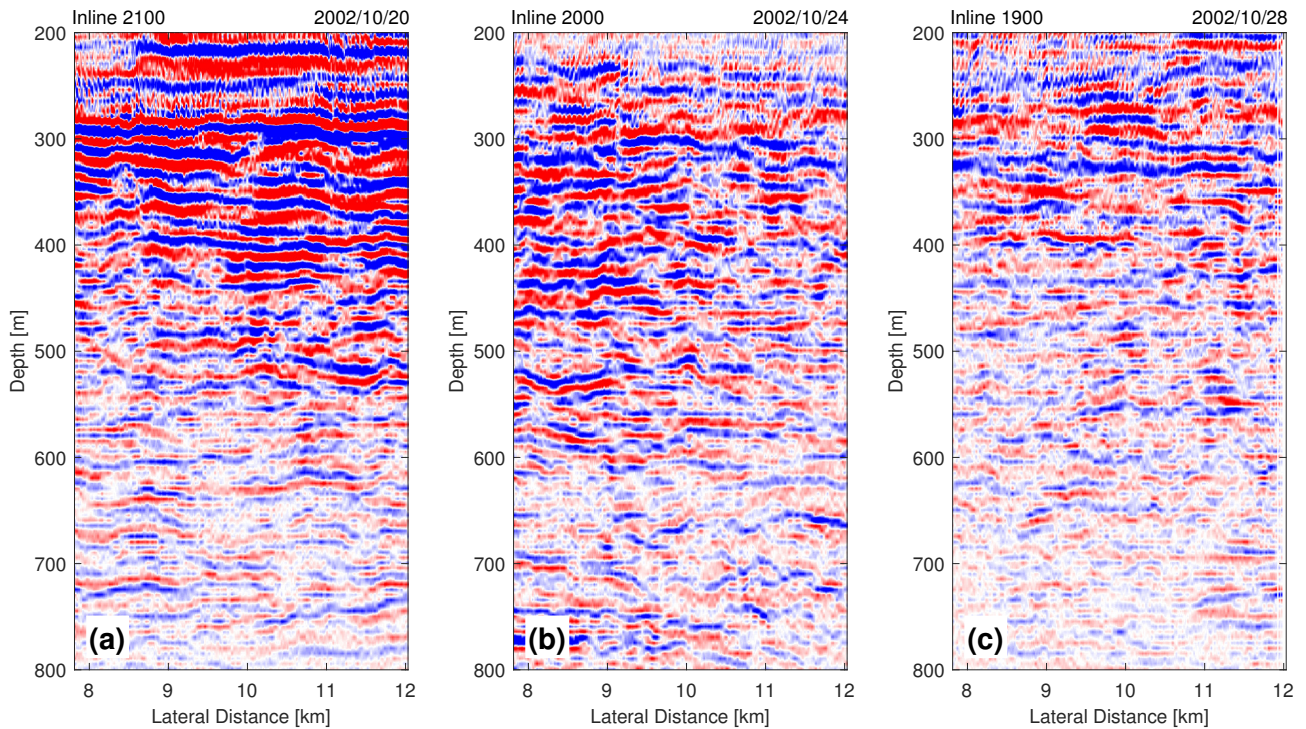
Figure 5. Three seismic inline images illustrating temporal variation of the water column. (a) IL # 2100; (b) IL # 2000; (c) IL # 1900. Inline numbers and the date of collection are noted on the top. Temporal and spatial separation between images is 4 days and 2.5 km, respectively.

In this section, we present multi-directional images from our 3D seismic volume to improve the understanding of water-column 3D seismic images and the fundamentals of 3D seismic oceanography, and hopefully, shed a light on possible ocean dynamics
175 that can be resolved from our seismic images.

Figure 5 shows three inline seismic images, each representing a snapshot along an inline transect in the linear acquisition period. We observe layers of strong seismic reflection in Fig. 5(a), moderate reflection in Fig. 5(b), and weak reflection in Fig. 5(c), respectively, indicating vertical temperature gradients of the water column (see Sec. 2.4). Considering the spatial (2.5 km) and temporal (about 4 days) separations in these images, we observe that the water-column structures varied, not only spatially
180 (over 5 km), but more importantly, temporally (over 8 days), suggesting a strong water-column mixing process may have occurred in this region. In other words, during the interval between October 20-28, 2002, over this portion (about 4 km) of the continental slope, the strong and thick thermoclines gradually weakened and thinned, and eventually almost disappeared. We interpret the water-column variation as complex and diverse internal wave variation over the continental slope of the northern Gulf of Mexico, caused by a time-varying mesoscale oceanographic process (length > 10 km, depth > 800 m, time > 10
185 days) which transformed the water column from highly stratified to well-mixed. The possible mesoscale processes causing this transformation will be further discussed in Sec. 4.
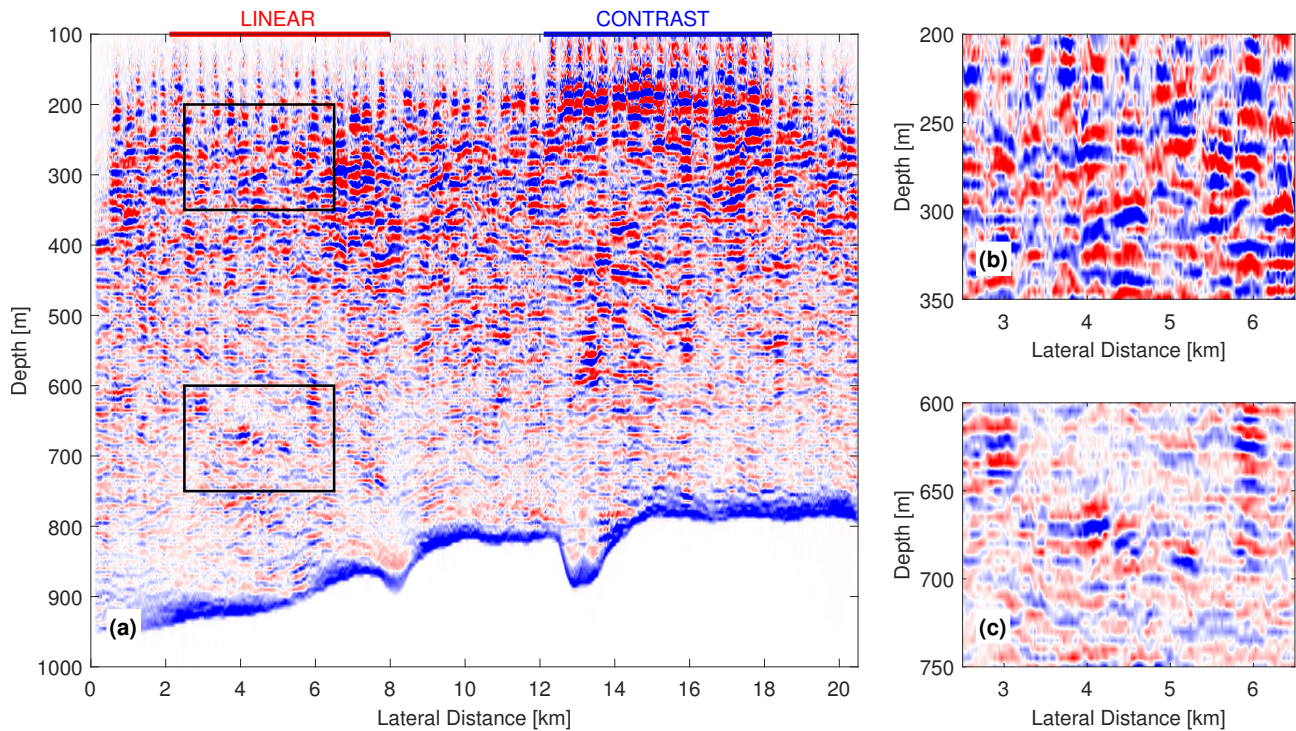
Figure 6. (a) An example of a crossline image (Crossline # 18200). (b) and (c) are close-up views of the regions shown in (a) for two different depths. The dates to collect the data span from August 2002 to February 2003. The red line at top marks the linear acquisition period, while the blue line marks the contrast period.

Figure 6 shows one of the widest crossline seismic images in our seismic area. We observe significant discontinuities and a strong pattern of seismic swaths (e.g., vertical stripes). These discontinuities stem from abrupt changes of isopycnal depth (e.g., "heaving" of isopycnals) across seismic swaths, indicating the occurrence of temporal variation in the water column. In this

190 region, the ocean dynamics that may change isopycnal depths include eddies, internal waves, internal tides, and Mississippi River outflow. Swaths collected over the linear acquisition period (marked by the red line) display some continuity, while swaths collected with longer time shifts can yield significant discontinuities. For example, seismic imaging of the contrast acquisition period (marked by the blue line) looks drastically different from its neighboring parts due to a 20-day time shift (see Fig. 4). We also notice that the discontinuity varies with depth. The discontinuity is more significant at 200-350 m [Fig. 6(b)] than

195 at 600-750 m [Fig. 6(c)], suggesting that temporal variation is more significant at shallower depths. Another proof for the discontinuity indicating temporal variation is the continuous seafloor, suggesting no temporal variation. Our analysis suggests that temporal variation of the water column, appearing as imaging discontinuity, is significant along the crossline direction, which lowers the quality of crossline images, and may further hinder their interpretation.

Figure 7 shows depth-slice seismic images at three different depths (250, 500, and 750 m) to represent the shallow, middle,

200 and deep layers of our seismic volume. Water-column seismic depth slices are the most complex representation to conceptu-
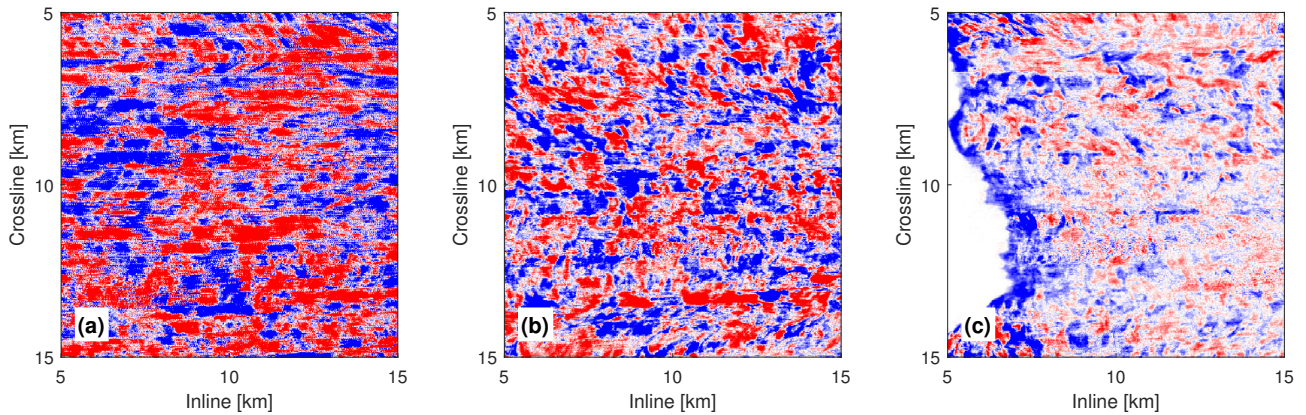
Figure 7. Seismic depth-slice images at three depths: (a) 250 m; (b) 500 m; (c) 750 m. The two axes shows the lateral distance in inline and crossline directions, respectively.

alize since they offer a new view of the ocean interior. We observe little discontinuity along the inline direction, suggesting that temporal variation is weak along the inline direction. However, we observe significant swath pattern and strong discontinuity appearing along the crossline direction, and the discontinuity decreases from shallow to deep layers. This decreased discontinuity agrees with the fact that temporal variability of the top ocean is more significant than that of the deep ocean, as the ocean is mainly stirred from the top due to the wind-driven surface mixing (Talley et al., 2012). Due to the presence of temporal variation, interpreting seismic depth-slice images is extremely challenging, but we may get a hint on the timescale of the ocean dynamics in Fig. 7, based on the amount of discontinuities and our 3D seismic setup (e.g., time separation between nearby seismic swaths). We suggest that in this region, the ocean dynamics have a timescale less than 8 hours at the depth of 250 m, but way longer than 8 hours at 750 m. The analysis of depth-slice images suggests that in our seismic volume, temporal variation of the water column is non-negligible in the crossline direction but negligible in the inline direction.

Our analysis of 3D seismic images reveals that temporal and spatial variations are both embedded in the seismic volume, and temporal variation is mostly along the crossline direction. Next, we will conduct analyses to quantitatively assess temporal and spatial variations within a 3D ocean seismic volume.

3.2 Theoretical Analysis

Here is a simple theoretical example to help us understand why temporal variation appears differently in inline and crossline directions. Let us assume a water column in which temporal variation occurs at one cycle per day (1 cpd, about 10^{-5} Hz) and spatial variation at one cycle per kilometer (10^{-3} cpm). The values here are arbitrary but can represent mesoscale oceanographic processes such as internal waves or internal tides (Talley et al., 2012) for which seismic imaging is particularly useful. We use single-frequency variations here for easy illustration purposes, while more complex variations can be viewed as the sum of multiple single-frequency variations. For simplification, we will refer to the total variation (sum of temporal and spatial variations) in the inline direction as *inline variation*, and the total variation in the crossline direction as *crossline variation*.
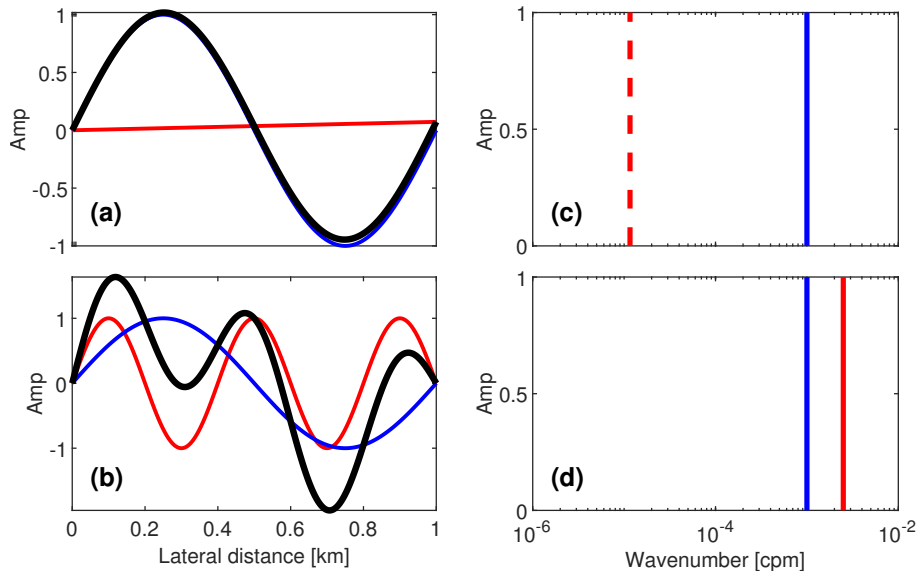
Figure 8. Illustration of temporal (red), spatial (blue) and total (black) variations in inline and crossline directions for a simple water column. (a) inline variation; (b) crossline variation; (c) spectrum of inline variation; (d) spectrum of crossline variation. Note that the dash line in (c) marked the theoretical position of temporal variations, which may not be resolved due to collection time.

We assume that this water column is imaged with a common 3D seismic survey setup, having the same field geometry of our survey, and carried out swath-by-swath like the linear acquisition period. The vessel sails at a speed of 2 m/s, the seismic swath is 400 m wide, and the vessel can collect two swaths per day. Therefore, after accounting for the two-way travel time, surveying a 1-km inline section takes 10^3 s (about 0.012 days, or 0.012 temporal cycle), and surveying a 1-km crossline section takes 2.5 days (2.5 temporal cycles, or 2.16×10^5 s).

Based on the above settings, the inline and crossline variations can be theoretically resolved [Fig. 8 (a) and (b)], summing temporal and spatial variations in inline and crossline directions, respectively. Results suggest that in the inline direction [Fig. 8 (a)], temporal variation is subtle, and the inline variation mostly follows spatial variation. In the crossline direction [Fig. 8 (b)], however, temporal variation is prominent, and the crossline variation is a fair combination of both temporal and spatial variations, with temporal variation being more noticeable. Furthermore, we find that this conclusion can be extended to temporal and spatial variations for all ocean dynamics. This theoretical analysis confirms that with common 3D seismic survey setups, temporal variation of mesoscale ocean dynamics is more significant in the crossline direction. In terms of seismic imaging, inline images mostly represent spatial variation of the water column, while the crossline images represent a combination of temporal and spatial variations of the water column.

Finally, the inline and crossline variations can be spectrally analyzed using Fourier transform, to reveal the distribution of temporal and spatial components in wavenumber domains [Figs. 8 (c) and (d)]. Here, we focused on wavenumber domains instead of frequency domains because seismic images are originally intended to resolve spatial variation rather than temporal

variation. We found that the spatial component appears at the same location, e.g., at 10^{-3} cpm, in both directions, while the temporal component appears at two different locations, e.g., at about 10^{-5} cpm in the inline direction and 2.5×10^{-3} cpm in the crossline direction. In other words, in inline images, temporal variation will appear as a low-frequency component, far apart (about two orders, 100 times) from the spatial component, while in crossline images, temporal variation appears as a high-frequency component, very close (about 2.5 times, still in the same order) to the spatial component. The dashed line in the inline spectrum [Fig. 8 (c)] illustrates the theoretical position of the temporal component, which is too weak to resolve when inline sections are too short (i.e., covering far less than one temporal cycle). These spectral analyses suggests that water-column temporal variation will appear differently in inline and crossline images, posing strong high-frequency aliasing in the crossline imaging. Also, separating temporal and spatial variations in crossline imaging could be very challenging because they are spectrally close to each other.

3.3 Empirical Analysis

Our theoretical analysis provides an idea for quantitatively analyzing temporal and spatial variations based on inline and crossline variations. However, real 3D ocean seismic volumes are more complicated than single-frequency-variation examples. Here we developed a method to analyze temporal and spatial variations within our 3D seismic volume. The results will provide empirical values in our seismic volume, which can also be useful to other seismic oceanography studies with similar setups.

For a real 3D seismic volume, inline and crossline variations can be quantified with correlation, which measures the similarity between two variables or images. For 2D seismic images, x and y, the correlation is defined as:

$$r = \sum_{i,j} \frac{(x_{ij} - \overline{x})(y_{ij} - \overline{y})}{\sigma_x \sigma_y} \tag{2}$$

where, i and j form the 2D index, $\overline{x}$ and $\overline{y}$ are the means, and σ_x and σ_y are standard deviations of x and y. In practice, due to the perpendicular relationship between inline and crossline directions, the inline variation can be simply derived from correlation between crossline images [Fig. 9 (a)], while the crossline variation can be derived from correlation between inline images [Fig. 9 (b)].

We correlate the inline and crossline image series with corresponding reference images (IL #2140, or XL #18000), respectively. The correlations are plotted as functions of inline or crossline number. The inline axis can further be converted to lateral distances (spatial domain), while the crossline axis can be converted to both lateral distances (spatial domain) and acquisition time (temporal domain). The correlation results are between -1 and 1, representing the fluctuation of image similarity with respect to the reference, with +1 being exactly similar, -1 exactly reversed, and 0 completely different. When the water-column structure varies, either temporally or spatially, the similarity between seismic images varies as well. Therefore, the change of the image similarity summarizes the variation of the water column.

The correlation results allow quantitative analysis of the variation of a particular image series or at a particular depth range. For example, we only use the linear period (see Fig. 4) for a more meaningful analysis. To best represent the variation of water column, we only use imaging of 250-750 m, excluding seafloors and low-quality shallow portion data. Furthermore, we divide the water column into two parts, the upper part (250-500 m) and the lower part (500-750 m), to explore the depth dependency.
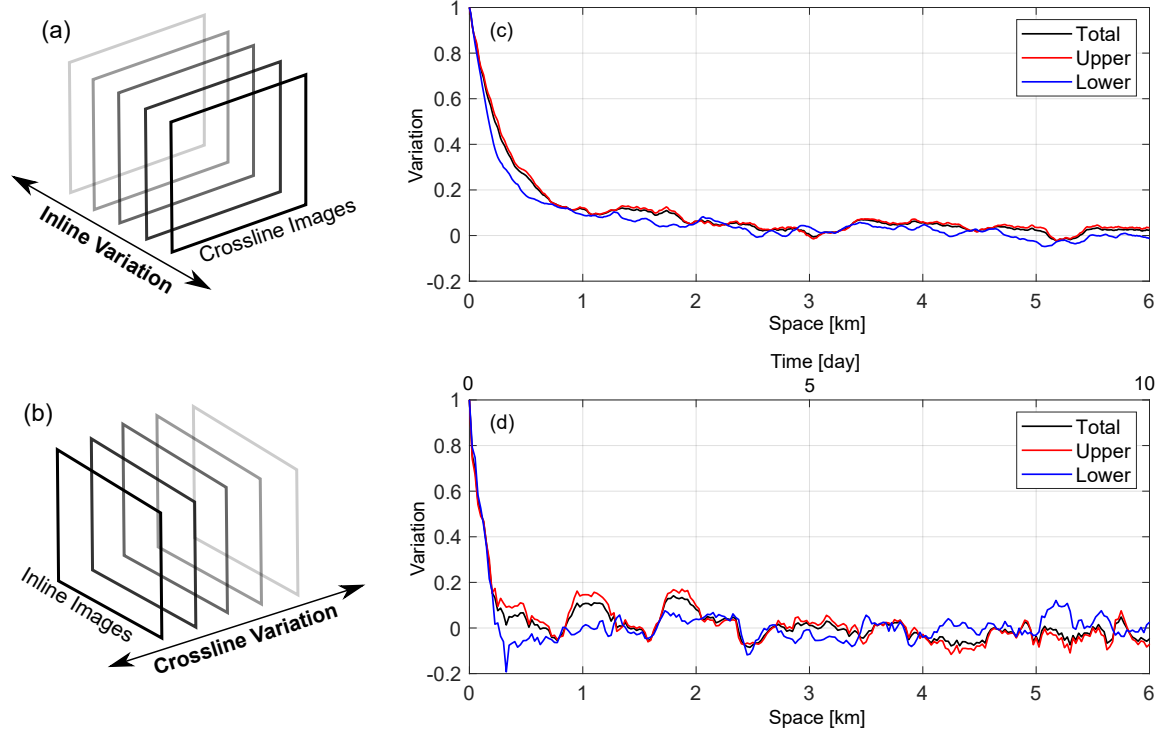
Figure 9. Inline and crossline variations from our seismic volume. Illustrations of (a) deriving inline variation from crossline image series, and (b) deriving crossline variation from inline image series. Results of (c) inline variation and (d) crossline variation. The red, blue and black curves are variations for the upper (250-500 m), lower (500-750 m) and total (250-750 m) water column, respectively. The crossline variation is calculated within the linear acquisition period (Inline 1900-2140, see Fig. 4). The time and space scales in (d) follow the linear acquisition period, which spans 6 km in space or 10 days in time (yielding a ratio of 0.6 km/day). The inline variation is limited to 6 km for easy comparison with the crossline.

Besides, the correlation function allows the examination of the correlation length, which is defined as the length to the first zero crossing, measuring the length required for two images to be completely different. The shorter the correlation length is, the faster the signal de-correlated. Finally, for periodical signals, the spectra of the correlation function can be used to study
275 the inherent cycles within the signal.

Figure 9 shows the results of inline and crossline variations derived from our 3D seismic volume. Here, inline variation [Fig. 9 (c)] is plotted as a function of space (i.e., lateral distance), while crossline variation [Fig. 9 (d)] is plotted as a function of space or time (based on the acquisition time). Overall, both inline and crossline variations quickly decrease from unity and then fluctuate around zero. The upper and lower water columns vary very differently, and the total variation of the whole
280 water column is mostly dominated by the upper part. Comparing these two directions, three observations can be made: (a) the crossline variation fluctuates more than the inline variation; (b) the crossline variation has a shorter correlation length (about
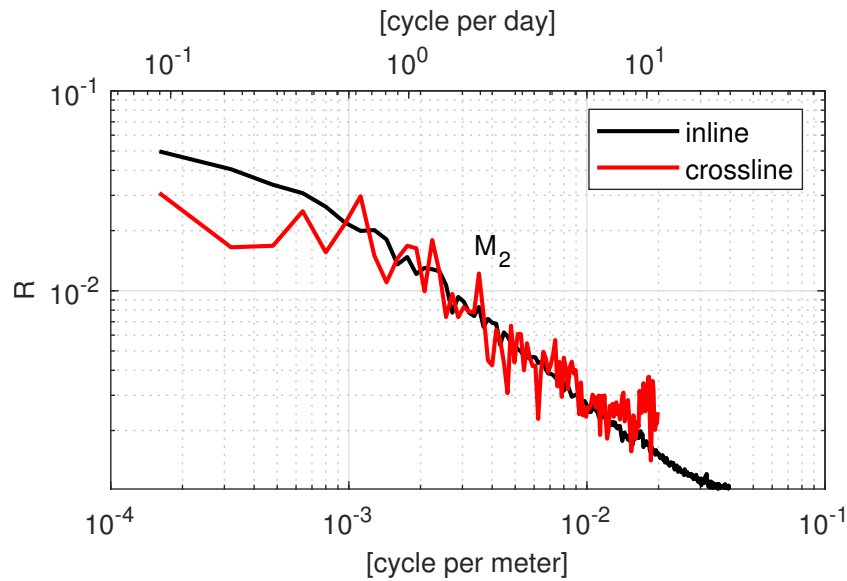
Figure 10. Inline and crossline spectra. The crossline spectrum is associated with both time and space cycles (with a ratio of 0.001666 cpm/cpd), calculated from Fourier transform of the crossline variation in time scale and and from that in space scales, respectively. The inline spectrum is only associated with the space cycle only, calculated from Fourier transform of the inline variation. The semi-diurnal (M2) tidal cycle is also denoted (at 2 cpd, or about 3.3×10^{-3} cpm in space scale).

0.4 km) than the inline variation (about 2.5 km); (c) the crossline variation has more high-frequency fluctuations than the inline variation. These observations can only be explained with the presence of temporal variation in crossline variation, leading to more and faster fluctuation and shorter correlation lengths, agreeing with our theoretical analysis [see Fig. 8 (a) and (b)]. Thus, our analysis confirms that in our 3D seismic volume, the inline variation [Fig. 9(c)] is mostly associated with spatial variation, while the crossline variation [Fig. 9(d)] is associated with both temporal and spatial variations.

Figure 10 further shows the inline and crossline spectra, calculated from the Fourier transform of the inline and crossline variations, respectively. Note that the inline is only associated with space, while the crossline is associated with both time and space. Overall, we observe a similar descending trend in both spectra, providing us information about the spatial features in wavenumber domains. Comparing these two spectra, one can see that many peaks seen in the crossline spectrum are absent in the inline spectrum. These peaks show the dominant frequencies of temporal variations. Particularly, we observe the semi-diurnal tidal cycle (marked as M_2 in Fig. 10) in the crossline spectrum, which is strong evidence that the crossline variation includes temporal variations, as continental marginal waters are often heavily influenced by tidal-forcing dynamics. A significant amount of high-frequency components seen in the crossline spectrum are temporal variation, agreeing with our theory [Fig. 8 (d)] which suggests that temporal variation appears as a high-frequency aliasing. Our spectral analysis, again, confirms that the crossline imaging captures temporal features of the ocean, while the inline imaging only captures the spatial features.

4   Discussion

The visual, theoretical, and data-driven analysis of the 3D seismic volume has provided a wealth of findings that we further discuss and summarize herein. Notice that this is a fairly new field, and we do not have a complete catalog of results and detailed concurrent oceanographic measurements that would allow unambiguous interpretation of the 3D seismic imaging in light of oceanographic processes.

Fundamentally, 3D seismic oceanography resolved from common 3D seismic survey setups will be intrinsically affected by temporal variations of ocean dynamics. Ideally it is possible to design a special 3D seismic survey that can perfectly image an oceanographic process without significant temporal variation. However, 3D seismic surveys are very expensive to collect and, in most of the case, we have to rely on data acquired for other purposes. 3D seismic surveys conducted for oil and gas exploration cover a very large volume of ocean water and have the right bandwidth to depict water column reflections. Those surveys often are acquired over time spanning from days to months, and we must look for the oceanographic signals embedded in the seismic data and build the best processing and analysis workflow to extract them. Mesoscale and sub-mesoscale ocean dynamics (e.g., fronts, eddies, internal waves, turbulence, etc) have frequencies 10^{-6}–10^2 Hz and wavenumbers 10^{-4}–10^2 cpm (Talley et al., 2012; Ruddick, 2018). As a result, wave spectra resulting from mismatched imaging inevitably produce a significant overlap of temporal variations on top of spatial variation. Temporal variation in 3D imaging may vary case by case, dataset by dataset, volume by volume.

In standard 3D seismic data processing for earth interior imaging, reflections within a large volume of subsurface are utilized and account for out-of-plane acoustic scattering, to provide higher quality images than those resulting from 2D data. The general rule is to avoid summing inconsistent reflections from different seismic swaths. This is not always possible for the water column due to temporal variation. Narrow aperture 3D multiparametric stacking (Bakhtiari Rad and Macelloni, 2020) or swath-by-swath common mid-point 3D stacking (Blacic and Holbrook, 2010) can both be used to create 3D seismic oceanographic images because both implement a time-dependent selection for the seismic data. However, the processing workflow for 3D seismic oceanography can be case-dependent, and we suggest always to perform an in-depth temporal analysis to avoid summing time-inconsistent seismic data.

Generally, we found that:

Inline images are not affected by temporal variation unless the inline is very long or is imaging fast-moving water-column structures (Klaeschen et al., 2009). Each inline can be seen as a snapshot of the water column vertical thermocline structure at a given time over a given location. This temporal and spatial heterogeneity cannot be fully separated because this temporal evolution occurs at different locations. However, available data analysis methods, e.g. wavefield spectral analysis (Holbrook et al., 2013) and diffusivity estimations (Fortin et al., 2017; Dickinson et al., 2017), developed for 2D seismic oceanography, can be safely extended to 3D inline images. Most importantly, because an inline section "samples" the ocean at one given time and one given place, we could have a particular sequence of inline images that adequately image both the spatial and temporal variations of oceanographic processes. This knowledge can be applied to understand time-evolving mesoscale ocean dynamics, e.g., eddies and internal waves, as the evolution of their vertical structures is very difficult to capture using traditional in-situ

oceanographic measurements. Recent 3D seismic oceanography studies with the time-lapsing concept (Dickinson et al., 2020; Gunn et al., 2020) are perfect examples of the application of this temporal variability in oceanographic studies. This temporal feature makes 3D seismic oceanography an extremely powerful tool for studying the temporal evolution of mesoscale ocean dynamics.

335   Crossline images capture both temporal and spatial information. Temporal variation being more prominent than spatial variation in the crossline direction is validated by the discontinuity in crossline images (Fig. 6), and by faster fluctuation in correlation function analysis in crossline direction (Fig. 9) and is verified by theoretical analysis [Figs. 8 (b), (d)]. In contrast, if temporal variation of an imaged structure is less prominent, it would be buried under spatial variation without showing any discontinuity in crossline imaging. For example, the seafloor appears highly continuous (does not exhibit temporal variations)

340   in our crossline imaging (Fig. 6) because it is associated with a long geological timescale longer than years. In general, ocean crossline images appear as low-quality seismic images, which might limit the imaging interpretation. This is mostly due to discontinuity induced by temporal variation, rather than fewer receivers in the crossline direction than in the inline direction (8 vs. 640). Therefore, the low quality cannot be improved through common processing techniques such as trace interpolation (Yilmaz, 2001). Instead, the crossline imaging can only be improved by optimized 3D seismic survey configurations specifically

345   designed for seismic oceanography, e.g., faster data collection across swaths in the crossline direction. Nevertheless, crossline images still provide valuable information, offering an immediate overview of the temporal distribution of the seismic survey.

In depth-slice images, temporal variation only appears in the crossline direction and is highly depth-dependent. This depth dependency comes from the timescale of ocean dynamics that occur at different depths. Due to water mixing of surface wind-waves, the top portion of the water column is usually highly dynamic, while the deep water is associated with a very long

350   timescale (Talley et al., 2012). Such a depth dependence, in terms of imaging discontinuity, can be seen in the crossline images (Fig. 6) and depth-slice images (Fig. 7), which is also evidence of the presence of temporal variation in the crossline direction. This depth dependency in 3D seismic oceanography can be a useful indicator to study the timescale of ocean dynamics at different depths.

A full investigation of the ocean dynamics observed by our seismic images, which would require further analysis of concur-

355   rent in-situ measurements and satellite data, is beyond the scope of this study, and will be conducted in our future study. Here we briefly discuss mesoscale ocean processes apparent in our 3D seismic images. Prior studies show the water dynamics in this region are dominated by Loop Currents and Mississippi river outflows, and possible ocean dynamics may include river plumes, internal waves, internal tides, and eddies (Coleman, 1988; Sturges and Lugo-Fernandez, 2005; Hamilton and Lee, 2005). For clear inference from our seismic images (Figs. 5–7) an ocean process should have a temporal cycle longer than 8 days (the

360   time separation between seismic images), a length scale larger than 25 km (exceeding the maximum width of our seismic images), and a depth of influence down to 800 m (generating internal wave field near the seafloor). Cross-referencing the above scales with the typical scales of possible ocean dynamics in this region, the only matched ocean dynamics are eddies. The Loop Currents create omnipresent cyclonic and anticyclonic eddies, moving northward and eastward in the Gulf of Mexico. We suggest that our seismic images have captured the process of an eddy approaching to the northern continental slope. When

365   eddies approach the continental margin, they start to interact with the continental slope and generate internal wave fields over

the slope. This process increases the vertical mixing and reduces the stratification, leading to a change of the water column from highly stratified to well-mixed (as seen in Fig. 5).

5 Conclusions

This study focuses on providing fundamental understanding of spatial and temporal variations embedded in 3D seismic data collected for oil and gas exploration. A 3D seismic volume of the northern Gulf of Mexico water column has been presented, and temporal and spatial variation in 3D oceanic seismic volume have been investigated for the first time using theoretical analysis and a correlation-based data analysis. Our results shows that in common 3D seismic surveys, temporal variation of mesoscale ocean dynamics can show up in the crossline direction, allowing one to view individual inline images as time-lapsing snapshots. The crossline and depth-slice images are heavily affected by temporal variation, and they cannot be directly interpreted. This fundamental understanding is essential for the interpretation and analysis of 3D oceanic seismic images. It allows the extension of previous 2D seismic oceanography analysis, such as wave spectral analysis and diffusivity estimations, to 3D inline images, and to study the evolution of time-varying mesoscale ocean dynamics. The correlation analysis proposed in this study is an effective tool to access the temporal and spatial information within the seismic volume. We suggest that it is important to analyze temporal variation within a 3D seismic volume before the interpretation of 3D seismic images and the analysis of wave fields in the seismic images. We believe 3D oil industry seismic data carry a wealth of oceanographic information, and our future 3D seismic oceanography research will focus on further investigation of the evolution of mesoscale ocean dynamics (eddies and internal waves) in the northern Gulf of Mexico.

Data availability. The seismic data for this project were provided by Schlumberger WesternGeco. The data are available from Schlumberger Multiclient Seismic Data Library (http://www.multiclient.slb.com; area MC-14Q).

Author contributions. ZZ and LZ conducted seismic imaging analysis. PBR and LM performed 3D seismic data processing and imaging. All the authors equally contribute in writing and editing the manuscript.

Competing interests. The authors declare that they have no conflict of interest.

Acknowledgements. We would like to thank Schlumberger WesternGeco for providing the 3D seismic data. The seismic data were processed with software Vista from Schlumberger, Kingdom by IHS Markit, Seismic Unix from Colorado School of Mines. The 3D CRS program used in this study was developed by the Wave Inversion Technology (WIT) Consortium, Hamburg, Germany. This work was supported by the National Oceanic and Atmospheric Administration, Office for Ocean Exploration and Research (NOAA-OER) grant (NA17OAR011021).

References

Bakhtiari Rad, P. and Macelloni, L.: Improving 3D water column seismic imaging using the Common Reflection Surface method, Journal of Applied Geophysics, 179, 104 072, https://doi.org/10.1016/j.jappgeo.2020.104072, 2020.

Blacic, T. M. and Holbrook, W. S.: First images and orientation of fine structure from a 3-D seismic oceanography data set, Ocean Science, 6, 431–439, https://doi.org/10.5194/os-6-431-2010, 2010.

Buffett, G. G., Krahmann, G., Klaeschen, D., Schroeder, K., Sallarès, V., Papenberg, C., Ranero, C. R., and Zitellini, N.: Seismic oceanography in the Tyrrhenian Sea: thermohaline staircases, eddies, and internal waves, Journal of Geophysical Research: Oceans, 122, 8503–8523, https://doi.org/10.1002/2017JC012726, 2017.

Coleman, J. M.: Dynamic changes and processes in the Mississippi River delta, Geological Society of America Bulletin, 100, 999–1015, 1988.

Dickinson, A., White, N. J., and Caulfield, C. P.: Spatial variation of diapycnal diffusivity estimated from seismic imaging of internal wave field, Gulf of Mexico, Journal of Geophysical Research: Oceans, 122, 9827–9854, https://doi.org/10.1002/2017JC013352, 2017.

Dickinson, A., White, N. J., and Caulfield, C. P.: Time-Lapse Acoustic Imaging of Mesoscale and Fine-Scale Variability within the Faroe-Shetland Channel, Journal of Geophysical Research: Oceans, https://doi.org/10.1029/2019jc015861, 2020.

Fortin, W. F., Holbrook, W. S., and Schmitt, R. W.: Mapping turbulent diffusivity associated with oceanic internal lee waves offshore Costa Rica, Ocean Science, 12, 601–612, https://doi.org/10.5194/os-12-601-2016, 2016.

Fortin, W. F., Holbrook, W. S., and Schmitt, R. W.: Seismic estimates of turbulent diffusivity and evidence of nonlinear internal wave forcing by geometric resonance in the South China Sea, Journal of Geophysical Research: Oceans, 122, 8063–8078, https://doi.org/10.1002/2017JC012690, 2017.

Gorman, A. R., Smillie, M. W., Cooper, J. K., Bowman, M. H., Vennell, R., Holbrook, W. S., and Frew, R.: Seismic characterization of oceanic water masses, water mass boundaries, and mesoscale eddies SE of New Zealand, Journal of Geophysical Research: Oceans, 123, 1519–1532, https://doi.org/10.1002/2017JC013459, 2018.

Gunn, K. L., White, N., and Caulfield, C. c. P.: Time-Lapse Seismic Imaging of Oceanic Fronts and Transient Lenses Within South Atlantic Ocean, Journal of Geophysical Research: Oceans, 125, 1–26, https://doi.org/10.1029/2020JC016293, 2020.

Hamilton, P. and Lee, T. N.: Eddies and jets over the slope of the northeast Gulf of Mexico, in: Circulation in the Gulf of Mexico, pp. 123–142, The American Geological Union, Washington DC, 2005.

Holbrook, W. S. and Fer, I.: Ocean internal wave spectra inferred from seismic reflection transects, Geophysical Research Letters, 32, 2–5, https://doi.org/10.1029/2005GL023733, 2005.

Holbrook, W. S., Páramo, P., Pearse, S., and Schmitt, R. W.: Thermohaline fine structure in an oceanographic front from seismic reflection profiling, Science, 301, 821–824, https://doi.org/10.1126/science.1085116, 2003.

Holbrook, W. S., Fer, I., and Schmitt, R. W.: Images of internal tides near the Norwegian continental slope, Geophysical Research Letters, 36, 1–5, https://doi.org/10.1029/2009GL038909, 2009.

Holbrook, W. S., Fer, I., Schmitt, R. W., Lizarralde, D., Klymak, J. M., Helfrich, L. C., and Kubichek, R.: Estimating oceanic turbulence dissipation from seismic images, Journal of Atmospheric and Oceanic Technology, 30, 1767–1788, https://doi.org/10.1175/JTECH-D-12-00140.1, 2013.

Kinsler, L. E., Frey, A. R., Coppens, A. B., and Sanders, J. V.: Fundamentals of acoustics, Fundamentals of Acoustics, 4th Edition, by Lawrence E. Kinsler, Austin R. Frey, Alan B. Coppens, James V. Sanders, pp. 560. ISBN 0-471-84789-5. Wiley-VCH, December 1999., p. 560, 1999.

430   Klaeschen, D., Hobbs, R. W., Krahmann, G., Papenberg, C., and Vsemirnova, E.: Estimating movement of reflectors in the water column using seismic oceanography, Geophysical Research Letters, 36, https://doi.org/10.1029/2009GL038973, http://doi.wiley.com/10.1029/2009GL038973, 2009.

Lonergan, L. and White, N.: Three-dimensional seismic imaging of a dynamic Earth, Society, The Royal Transactions, Philosophical Sciences, Engineering, 357, 3359–3375, 1999.

435   Nakamura, Y., Noguchi, T., Tsuji, T., Itoh, S., Niino, H., and Matsuoka, T.: Simultaneous seismic reflection and physical oceanographic observations of oceanic fine structure in the Kuroshio extension front, Geophysical Research Letters, 33, 1–5, https://doi.org/10.1029/2006GL027437, 2006.

Nandi, P., Holbrook, W. S., Pearse, S., Páramo, P., and Schmitt, R. W.: Seismic reflection imaging of water mass boundaries in the Norwegian Sea, Geophysical Research Letters, 31, 1–4, https://doi.org/10.1029/2004GL021325, 2004.

440   Piété, H., Marié, L., Marsset, B., Thomas, Y., and Gutscher, M. A.: Seismic reflection imaging of shallow oceanographic structures, Journal of Geophysical Research: Oceans, 118, 2329–2344, https://doi.org/10.1002/jgrc.20156, 2013.

Ruddick, B. B., Song, H., Dong, C., and Pinheiro, L.: Water column seismic images as maps of temperature gradient, Oceanography, 22, 192–205, https://doi.org/10.5670/oceanog.2009.19, 2009.

Ruddick, B. R.: Seismic oceanography's failure to flourish: a possible solution, Journal of Geophysical Research: Oceans, 123, 4–7,
445   https://doi.org/10.1002/2017JC013736, 2018.

Sallarès, V., Biescas, B., Buffett, G., Carbonell, R., Dañobeitia, J. J., and Pelegrí, J. L.: Relative contribution of temperature and salinity to ocean acoustic reflectivity, Geophysical Research Letters, 36, 1–6, https://doi.org/10.1029/2009GL040187, 2009.

Sheen, K. L., White, N., Caulfield, C. P., and Hobbs, R. W.: Estimating Geostrophic Shear from Seismic Images of Oceanic Structure, Journal of Atmospheric and Oceanic Technology, 28, 1149–1154, https://doi.org/10.1175/JTECH-D-10-05012.1, 2011.

450   Song, H. B., Pinheiro, L., Wang, D. X., Dong, C. Z., Song, Y., and Bai, Y.: Seismic images of ocean meso-scale eddies and internal waves, Chinese Journal Of Geophysics-Chinese Edition, 52, 2775–2780, https://doi.org/10.3969/j.issn.0001-5733.2009.11.012, 2009.

Sturges, W. and Lugo-Fernandez, A., eds.: Circulation in the Gulf of Mexico: Observations and Models, Geophysical Monograph Series, American Geophysical Union, Washington, D. C., https://doi.org/10.1029/GM161, http://doi.wiley.com/10.1029/GM161, 2005.

Talley, L. D., Pickard, G. L., Emery, W. J., and Swift, J. H.: Descriptive Physical Oceanography, Elsevier, 6th edn., 2012.

455   Tang, Q., Wang, C., Wang, D., and Pawlowicz, R.: Seismic, satellite, and site observations of internal solitary waves in the NE South China Sea, Scientific Reports, 4, 1–5, https://doi.org/10.1038/srep05374, 2014a.

Tang, Q. S., Gulick, S. P. S., and Sun, L. T.: Seismic observations from a Yakutat eddy in the northern Gulf of Alaska, Journal of Geophysical Research: Oceans, 119, 3535–3547, https://doi.org/10.1002/2014JC009938, 2014b.

Yilmaz, Ö.: Seismic data analysis: Processing, inversion, and interpretation of seismic data, Society of Exploration Geophysicists, 2001.